Decoding the vertical phase separation and its impact on C8-BTBT/PS transistors properties

Ana Pérez-Rodríguez[1], Inés Temiño[1], Carmen Ocal[1], Marta Mas-Torrent[1,2], Esther Barrena[1*]*

[1]Institut de Ciència de Materials de Barcelona (ICMAB-CSIC), Campus de la UAB, 08193 Bellaterra, Spain.

[2]CIBER-BBN, Campus de la UAB, 08193 Bellaterra, Spain.

* ebarrena@icmab.es

* mmas@icmab.es

KEYWORDS: Organic semiconductors, friction anisotropy, AFM, OFETs, C8-BTBT

ABSTRACT

Disentangling the details of the vertical distribution of the small semiconductor molecules blended with polystyrene (PS) and the contacts properties are issues of fundamental value for designing strategies to optimize small molecule/polymer blend organic transistors. These questions are addressed here for ultra-thin blends of 2,7-dioctyl[1]benzothieno[3,2-b][1]benzothiophene (C8-BTBT) and PS processed by a solution-shearing technique using three different blend composition ratios. We show that friction force microscopy (FFM) allows the determination of the lateral and vertical distribution of the two materials at the nanoscale. Our results demonstrate a three layer stratification of the blend: a film of C8-BTBT of few molecular layers with crystalline order sandwiched between a PS-rich layer at the bottom (a few nm thick) acting as passivating dielectric layer and a PS-rich skin layer on the top (~1nm) conferring stability to the devices. Kelvin probe force microscopy (KPFM) measurements performed in operating organic field-effect transistors (OFETs) reveal that the devices are strongly contact limited and suggest contact doping as route for device optimization. By excluding the effect of the contacts, field-effect mobility values in the channel as high as 10 $cm^2V^{-1}s^{-1}$ are obtained. Our findings, obtained via a combination of FFM and KPFM, provide a satisfactory explanation of the different electrical performance of the OFETs as a function of the blend composition ratio and by doping the contacts.

INTRODUCTION

Organic field-effect transistors (OFETs) have been widely studied because of their potential in a wide range of applications such as printable and flexible electronics. Organic semiconductors (OSCs) are especially interesting owing to their compatibility with solution-based coating techniques, which promise low-cost manufacturing by high-throughput continuous roll-to-roll printing methods on flexible substrates.[1] Over the past years intensive research efforts from both academia and industry have been performed for achieving superior performance of OFETs processed with solution-based coating techniques. As organic semiconducting polymers are generally less crystalline than small molecules and, as a result, tend to exhibit lower carrier mobility,[2] many efforts have been devoted to develop soluble small conjugated molecules. However, the processing of small molecules from solution encounters coating problems related with dewetting and lack of control over the nucleation and growth of the molecular crystallites.[3,4] Therefore, obtaining highly reproducible and uniform crystalline films by solution-coating is challenging for many molecular systems and, as a consequence, large performance disparity among devices is obtained even on the same substrate type.[4,5] One of the advances in the solution-manufacturing process is raised from the idea of blending small conjugated semiconductor molecules with an amorphous insulating polymer to benefit from the advantages of both types of materials: uniform film-forming properties from the polymer component and high carrier mobility from the small molecule component.[1,3,6–9] This strategy has led to an overall rise in charge carrier mobility accompanied by an improvement of devices processability, reproducibility and stability.[1,8,10,11]

A key to understand the superior performance of OFETs fabricated with blended films seems to be the vertical phase separation of the two material components, previously confirmed by *ex situ* measurements, such as transmission electron microscopy (TEM),[12,13] secondary ion mass spectrometry[14] and neutron scattering[15] or variable angle spectroscopic ellipsometry.[15] Thus, discerning the structural details of the vertical stratification of the blends and the way it changes as a function of different processing parameters is an issue of fundamental importance.

Successful demonstration of OFETs based on small molecule/polymer blends have been reported for Cn-BTBT alkylated derivatives of benzothieno, one of the most promising small semiconducting molecules because of their proven high hole mobility.[12,16–19] It has been reported that blending polystyrene (PS) with 2,7-dioctyl[1]benzothieno[3,2-b][1]benzothiophene (C8-BTBT) enhances the device to device reproducibility, as well as improves the already remarkable stability of single component C8-BTBT films.[1] Moreover, lines of evidences of the vertical phase separation of both components, with PS segregated to the dielectric/semiconductor interface have been provided by cross-sectional TEM.[12] A bottom PS layer (in which a small percentage of C8-BTBT cannot be excluded) is believed to ensure a low density of traps at the semiconductor/dielectric interface.[1,8] Nevertheless, the detailed structure of the films at the nanometer scale has not been fully determined yet. This important question is addressed here for blends processed by a solution-shearing technique[8] for three C8-BTBT: PS ratios (1:2, 1:1 and 4:1 in weight). We show that lateral force imaging, also known as friction force microscopy (FFM) is a powerful tool to distinguish between C8-BTBT and PS regions thanks to the different frictional behaviors of these two materials. This fact allows obtaining a complete nanoscale characterization of the vertical distribution and crystalline quality of the blend components. The

resulting structure of the films correlates with the different macroscopic electrical performances of the OFETs obtained for the three blend ratios.

To understand the factors currently limiting transport in the most optimized devices, Kelvin probe force microscopy (KPFM) measurements in operating OFETs have been performed. We show that the devices are strongly limited by the contacts and that the incorporation of a doping interlayer of 2,3,5,6-tetrafluoro-7,7,8,8-tetracyanoquinodimethane (F4-TCNQ) offers a route for contact optimization. By excluding the contacts resistance we obtain a field-effect mobility in the channel as high as 10 $cm^2V^{-1}s^{-1}$.

EXPERIMENTAL SECTION

Blend films were deposited by the bar-assisted meniscus shearing (BAMS) technique[1] (Figure 1b) in ambient conditions as described elsewhere.[1,8] The materials, C8-BTBT and PS (with molecular weight Mw = 10000 $g \cdot mol^{-1}$), were purchased from Sigma-Aldrich and used without further purification. Blend solutions of C8-BTBT and PS in chlorobenzene 2 wt% were prepared at different weight ratios: 1:2, 1:1 and 4:1. The M_w of the PS was selected following the previously published optimized conditions[1] and results in solutions with a good viscosity to be processed into homogenous films. The bottom gate substrates were Si/SiO_2 (200 nm SiO_2) from Si-Mat, and they were cleaned with high purity acetone and isopropanol and then dried under a nitrogen flux. The electrodes consisted of 7 nm of MoO_3 and 35 nm of gold deposited by metal evaporation through a shadow mask (channel lengths from L=30-100 μm and channel width of W=4 mm) in the configuration shown in Figure 1c.

Electrical measurements were performed in ambient conditions using an Agilent B1500A semiconductor device analyser connected to the samples with a Karl Süss probe station. The field-effect mobility in the saturation regime was extracted using the relationship:

$$\mu = \frac{2L}{WC_i} \times \left(\frac{\partial\sqrt{I_{SD,sat}}}{\partial V_{SG}}\right)^2 \quad (1)$$

where C_i is the insulator capacitance per unit area, and W and L are the width and length of the channel, respectively. Atomic force microscopy (AFM) measurements were carried out at room temperature using a commercial head and control unit from Nanotec Electrónica S.L. All data were analysed with the WSxM freeware.[20] The contact mode FFM[21,22] study was carried out using Si tips mounted in soft ($k \approx 0.01$-0.1 Nm^{-1}) cantilevers from Veeco. Unless otherwise indicated, the load was always kept as low as possible (close to the pull off force) during FFM scanning. In KPFM the electrostatic force is nullified at each surface point and provides a map of local contact potential difference (CPD) values. We used the frequency modulation mode (FM-KPFM), in which the tip is excited by an ac voltage (~ 0.5 V) at a frequency (~ 0.7 kHz) while a feedback loop adjusts the dc bias needed to nullify the frequency shift (Δf) of the cantilever mechanical oscillation, which is proportional to the electrostatic force gradient.[23] In our set-up, the voltage is applied to the tip, so that the higher the local CPD the lower the local effective work function.[24] The CPD maps are obtained simultaneously with the topography in a single pass. For the FM-KPFM measurements, CrPt coated Si tips in cantilevers with nominal $k = 3$ Nm^{-1} from BudgetSensors were used. The error in the estimated channel mobility was obtained by error propagation from equation (2) taking into account the uncertainty in the determination of CPD.

RESULTS

Electrical Characteristics and Vertical Phase Separation.

Representative transfer curves of the three devices (with a 30 µm channel length) are shown in Figure 1d. The reproducibility of the devices was significant for the 4:1 ratio, with an average hole field-effect mobility of 0.3 $cm^2V^{-1}s^{-1}$.[1] The reproducibility of the devices was significant for this ratio, with over 90% devices showing a good performance. For the 1:1 ratio, the reproducibility dropped around 80%, and for 1:2 it reached 50%. The performance of the latter formulations also diminishes with respect to the 4:1 ratio up to 1 order of magnitude.

Studying the OFET electrical properties as a function of the blend ratio is a good systematic procedure to analyze the vertical phase separation taking place in each film and thus understand its impact on the electrical properties of the devices.

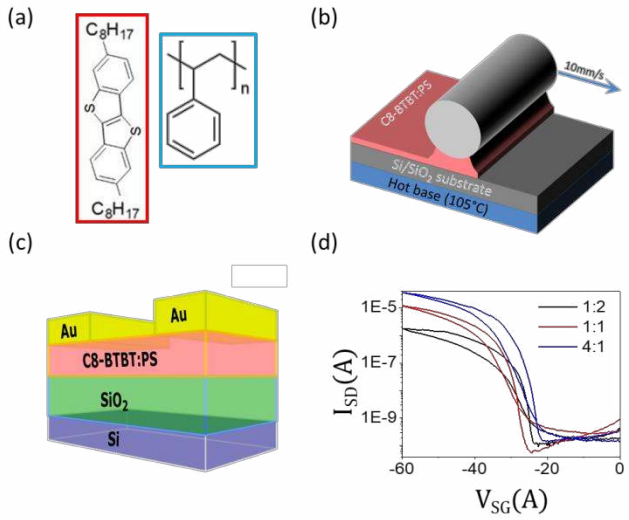

Figure 1. (a) Chemical structures of C8-BTBT and PS. (b) Schematic illustration of the BAMS technique. (c) Scheme of the geometry of the devices. (d) Representative transfer curves corresponding to the OFETs for the 1:2, 1:1, and 4:1 i ratios of C8-BTBT:PS (V_{SD}= –40V).

Although for the 1:2 device the optical images reflect significantly smaller crystal domains, the topographic AFM images show very similar features for the three investigated blend ratios (S1 in the Supporting Information), hampering the direct correlation between thin film morphology or crystallinity and electrical performance of the devices. Close inspection of the organic films topography inside the channel reveals a uniform and smooth surface consisting of large flat platforms or terraces with lateral sizes in the micrometer range. The height of each terrace is 3.1 ± 0.2 nm or multiples of it (S2 in Supporting Information) which is only slightly higher than the inter-planar distance of the reported C8-BTBT thin film structure consisting of a layered herringbone packing with the lamellar planes parallel to the surface. We note that this is the most favorable orientation for charge transport in OFETs.[19,25,26]

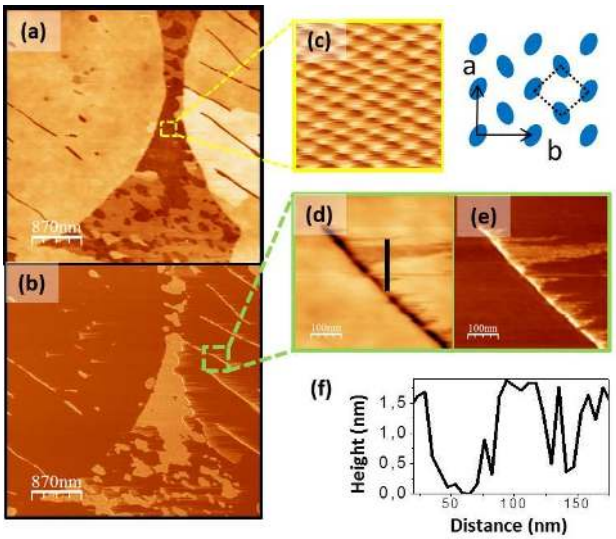

Figure 2. (a) Topographic and (b) lateral force images obtained within the channel of the 1:2 OFET. (L=30 µm) (c) Magnified molecular resolution image (5 nm x 5 nm) of C8-BTBT and top view model of the in-plane herringbone unit cell (*a*=0.59 nm, *b*=0.79 nm). Blue ellipsoids represent the methylene groups. (d) Topographic and (e) lateral force images obtained at the indicated area. (f) Profile along the black line traced in (d).

In the following, we focus on identifying the two different blend constituents, PS and C8-BTBT, based on a frictional response and crystallinity analysis. The investigation of the local frictional properties by means of FFM has shown to be a valuable tool to reveal structural details of molecular films which are difficult to visualize with other techniques.[22,27–30] Furthermore, on samples with a heterogeneous composition, the lateral force maps have been proven to be useful in identifying materials with a different chemical nature (such as graphene flakes[31,32] or organic islands on a substrate [33–35]) or to distinguish between two different chemical species in mixed self-assembled monolayers.[36] We first analyze the 1:2 ratio for which a substantial contrast between some areas is observed in the lateral force signal, where a darker color corresponds to lower friction. Figure 2a shows a topographic image and the simultaneously recorded lateral force taken on the device channel. On the terraces exhibiting the highest friction (lightest color), molecular-resolved images are obtained (Figure 2b) with an in-plane lattice constant ($\approx 0.6 \pm 0.1$ nm) in agreement with the next neighbors distance of C8-BTBT molecules in the herringbone packing within the plane (a=0.59 nm, b=0.78 nm),[19] evidencing the high crystalline quality of the C8-BTBT layer. Moreover, information about the phase separation is gained from the lateral force signal that allows relating the friction contrast with the material composition, that is, high friction for crystalline C8-BTBT and low friction for PS areas, respectively. As a matter of fact, molecular order is not observed on those terraces with low-friction as expected from the amorphous structure of PS. Interestingly, by consecutive scanning of these regions (or slightly increasing the imaging load) an extremely thin layer is peeled off by the swept action of the tip, leaving uncovered a surface exhibiting the friction contrast of C8-BTBT where molecular resolved images are obtained. This key observation permits firmly establishing the existence of an ultrathin skin layer of PS which covers large areas of the crystalline C8-BTBT. As can be

observed in the profile of Figure 2f, the thickness of the skin layer varies between 0.5 and 2 nm (further details in Figure S3 in Supporting Information). In addition, correlating topography and friction is particularly helpful for determining the vertical structure of the system, as there are regions of the channel where the C8-BTBT film is not complete but leaves exposed areas at lower vertical level. This is illustrated in Figure 3. Note, in particular, that the frictional signal of the base level terrace (Figure 3a), is lower than that of the surrounding C8-BTBT film and similar to that of the PS skin layer on the topmost level. In fact, no molecular order is attained at these regions suggesting a similar composition of skin and bottom layers, as confirmed next.

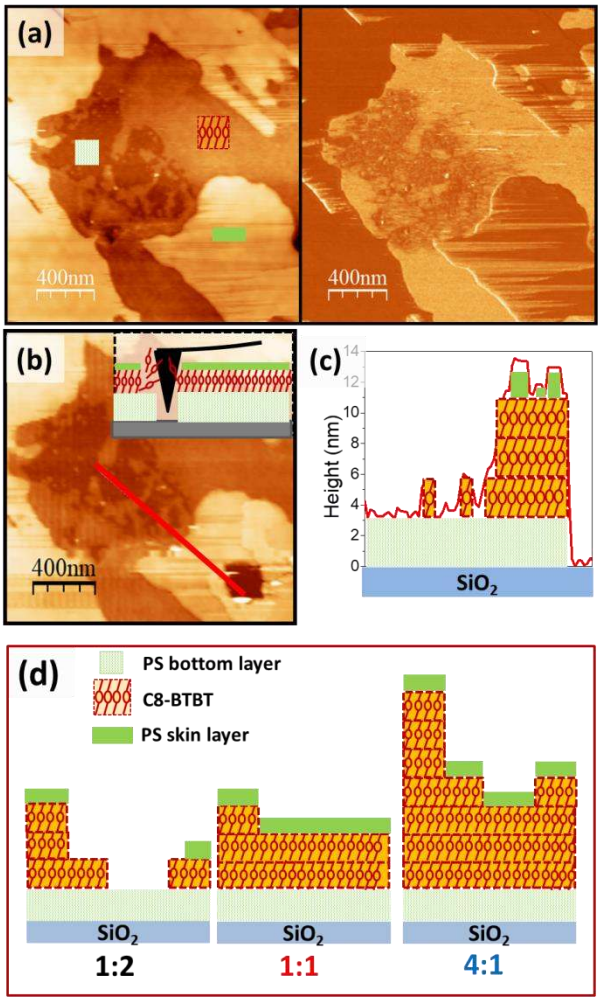

Figure 3. (a) Topography (left) and lateral force (right) images taken within the channel of a 1:2 OFET and (b) same area after scratching the film. Inset: Schematic illustration of the scratching experiments. (c) Relief profile (red line) along the segment marked in (b) and (d) deduced structure of the films for the three C8-BTBT:PS ratios.

To clarify whether the lowest level in Figure 3a corresponds to the substrate or to the presence of an underlying PS buffer layer, the film was locally scratched by scanning at a higher load (> 1 nN) till reaching the substrate (inset in Figure 3b). After this procedure, the same area was re-imaged at the released load revealing that scratching had led to a square cavity exposing the bare substrate. The uncovered SiO_2 serves as a reference to evaluate the thickness of the different layers as well as that of the overall film (Figure 3b). The height analysis confirms the existence of a layer of ~2-3 nm under the C8-BTBT film (profile in Figure 3c) identified by FFM as PS rich. We conclude that the films have a vertically phase separated structure consisting of a C8-BTBT crystalline film sandwiched between two PS layers at the bottom and on the top. The interface between the different layers is very smooth and structurally well defined. The segregation of PS at both interfaces, with SiO_2 and air, despite their dissimilar surface energy, suggests a phase separation driven by the crystallization of C8-BTBT rather than by surface energy minimization. The formation of a PS layer at the bottom has been suggested in the literature to serve as a nonpolar dielectric medium that assures low charge trapping between the dielectric and the OSC.[8,12,37] However, as far as we know, the presence of a skin layer on the top of the OSC has not yet been experimentally proven for this system.

Following the above described procedure we characterized the vertical distribution of PS and C8-BTBT with a nanometer precision for the samples prepared with diverse C8-BTBT:PS ratios

(1:2, 1:1 and 4:1). Although the films surface morphology has a similar appearance (see S1 in the Supporting Information) there are quantitative differences in the individual thickness of the three-layers of the structure, which are schematically summarized in Figure 3d. The total thickness determined for the 1:2, 1:1 and 4:1 ratios was ≈16, 13 and 25 nm, respectively.

It is noteworthy that for the 4:1 ratio, with the thickest C8-BTBT layer, the extracted current and mobility are the highest, whereas for the blends with 1:2, where not even a complete C8-BTBT layer is formed, a poor performance and lack of reproducibility were obtained.

Remarkably, the PS bottom layer and skin layer have the same thickness for all compositional ratios. Conversely, it is noticeable that, compared to the other ratios, in the case of the 1:2 blend, the C8-BTBT layer is the thinnest and consists of an incomplete C8-BTBT film, with a heterogeneous distribution of heights that leaves uncovered some areas of the bottom PS layer. For the other samples, the hole transporting layer consists of two complete C8-BTBT layers for the 1:1 ratio and three complete layers for the 4:1 ratio. Hence, we conclude that the ratio between the blend components affects the number of complete C8-BTBT crystalline layers formed, but it does not alter the thickness of both the bottom and top PS layers.

Role of PS in Films Stability

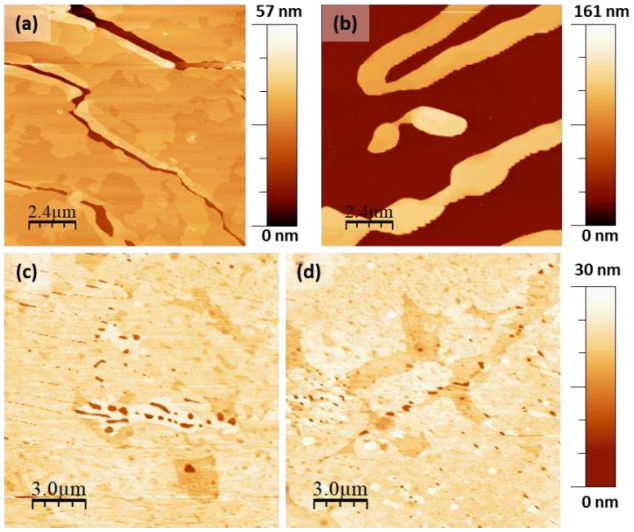

Figure 4. Topographic images of (a) freshly prepared C8-BTBT film (without PS), (b) same sample 4 months later, (c) freshly prepared C8-BTBT:PS film (4:1) and (d) same sample 14 months later.

To understand the role of the PS layers in possible aging, two types of samples were investigated by AFM as a function of time: the above described C8-BTBT:PS blend (4:1) and control samples processed under similar conditions but containing only C8-BTBT. Comparison of the very same samples (Figure 4), just as prepared (fresh) and after several months reveals that, in particular, the single component C8-BTBT films suffer from a strong dewetting with time. The initial 30 nm thick and laterally continuous films (Figure 4a) evolves to 90 nm high islands that leave uncovered large substrate regions (Figure 4b). Remarkably, for the C8-BTBT:PS blend, morphologically and structurally aging is negligible and the films present basically the same appearance at the nanoscale after more than one year from preparation (Figure 4c and 4d). It has already been reported that the hydrophobicity of the underlying PS buffer layer leads to an enhancement of the stability and reduces the trap density at the OSC-dielectric interface.[8,12,37] The present study suggests that the formation of both, top and bottom PS layers,

act as an encapsulation film for C8-BTBT impeding the dewetting of the C8-BTBT layers upon time.

KPFM under operation

Our results highlight that the C8-BTBT:PS blends have the basic ingredients to attain a high electrical performance: a crystalline film of C8-BTBT, favorably oriented for in-plane hole transport, sitting on top of a PS buffer layer acting as the passivating dielectric and encapsulated by an ultra-thin PS layer conferring stability to the devices. The measured C8-BTBT thickness for each device correlates with their different electrical performance (Figure 1d). To better understand the implications of the vertically phase-segregated structure on the device performance, we performed a KPFM nanoscale characterization of the OFETs under operation, as the CPD maps can shed light onto the charge transport and carrier injection.[38–41]

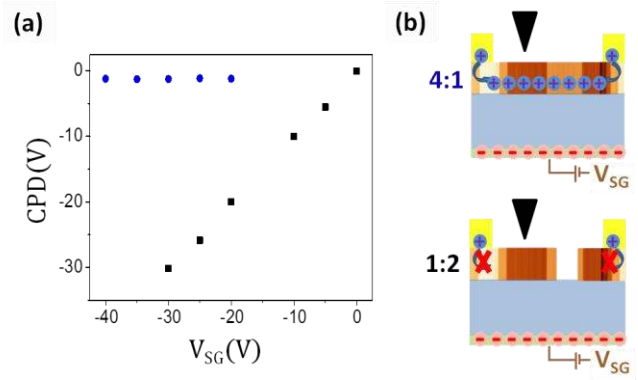

Figure 5. (a) CPD values inside the channel for V_{SD} = 0 upon applied V_{SG} bias for 1:2 and 4:1 OFETs and (b) schematic illustration of the formation or not of the charge accumulation channel upon V_{SG} application for 4:1 (top) and 1:2 (bottom) devices, respectively.

The formation or not of the accumulation layer of the OFETs can be locally evaluated by measuring the CPD within the channel as a function of the applied gate voltage (V_{SG}). To get information from the whole tri-layer structure (including the top and bottom PS layers), the measurements were performed at channel locations well away from any film void or topographic defect. The results are plotted in Figure 5a for OFETs with 1:2 and 4:1 blend ratios together with the schematics of the interpretation in terms of the formation or not of the charge accumulation channel. A completely different tendency is observed for each device. In device 1:2, the measured CPD coincides with V_{SG}, implying that no charges are injected into the device to screen the applied gate bias and, consequently, the charge accumulation channel is not formed (bottom cartoon in Figure 5b). This fact is directly related to the lateral discontinuity of the transport layer, consisting of an incomplete C8-BTBT film for this ratio. Additionally, in these devices, largely defective film coverage is also found at the electrodes boundary, which suggests the degradation of this C8-BTBT film upon evaporation of the electrodes (see S4 in the Supporting Information). These inhomogeneities at the OSC-electrode contact hinder to some extent the injection of charges needed to form the transport channel, however, there must be conductive paths connecting source and drain electrodes and making the device to work at macroscopic level although with low I_{SD} (see Figure 1d).

Conversely to the above description, devices based on the 4:1 blend show the expected behaviour for an operating OFET. In this case, the CPD in the channel does not change upon application of a gate bias, implying that charges are rapidly injected from the electrodes into the channel forming the accumulation layer that screens the gate bias (upper cartoon in Figure 5b).

It is, however, noteworthy that even for the optimal case of the 4:1 ratio, the hole field-effect mobility extracted from the transfer characteristics of the devices (0.3 $cm^2V^{-1}s^{-1}$ in average[1]) is lower than those reported in the literature for C8-BTBT OFETs.[12] One of the critical issues that can severely affect the OFET performance is the contact resistance between the metal electrodes and the semiconductor layer.[42] Determination of contacts resistance is found to be crucial in characterization of transistors as it may obscure mobility extraction. In the case of C8-BTBT, a hole injection barrier exists because of the large mismatch between the highest occupied molecular orbital (HOMO) and the work function of the gold electrode that is commonly ameliorated by using self-assembled monolayers (SAMs),[43] inserting a MoO_x layer,[44] doping the contacts[45,46] or using a metallic organic charge-transfer complex.[47] Figure 6a displays the representative CPD line profiles at two different V_{SD} values (V_{SD}= 0 V and V_{SD}= −5 V) and using a V_{SG}= −40 V for the OFET with a 4:1 ratio of the C8-BTBT:PS blend and in which a MoO_x layer has been incorporated underneath the Au contact (Au/MoO_x). As can be noticed from the CPD profile, microscopically the contact resistance (R_C) manifests by a sudden voltage drop at the source (marked in yellow) from which it can be extracted.

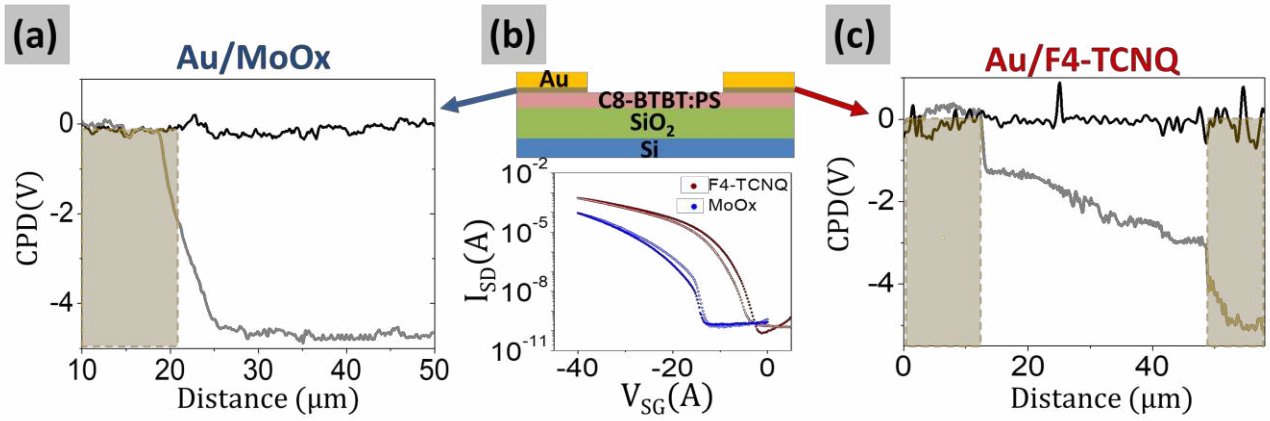

Figure 6. CPD profiles for V_{SD} = 0V and V_{SG} = –40V (black) and V_{SD} = – 5V and V_{SG} = –40V (grey) for C8-BTBT OFETs with 4:1 ratio using (a) Au/MoO_x and (c) the Au/F4-TCNQ contacts (L=40 μm). (b) Top: Schematics and transfer characteristics in the saturation regime of the devices fabricated with Au/MoO_x (in blue) and Au/F4-TCNQ (in red) contacts.

The ohmic behavior of the contact in this device was confirmed by the linear dependence of the CPD drop as a function of the applied V_{SD}, (Figure S5 in the Supporting Information). The extracted resistance at the source Au/MoO_x contact is $R_C \cdot W$ = 23.9kΩ·cm (OFET in the linear regime, V_{SD} = –5V and V_{SG} = –40V). The resistance in the channel estimated from the total resistance in the OFET is $R_{CH} \cdot W$ = 0.74 kΩ·cm, which gives evidence of a large relative contribution of the contact resistance and suggests a considerably higher charge mobility in the film than the effective mobility extracted from the current-voltage characteristics, following equation (1). Proven that the devices operation is strongly limited by the contacts, we have used F4-TCNQ as an interlayer (Au/F4-TCNQ) to improve the injection properties by means of its strong acceptor character enabling contact doping. On average from 11 devices, the switch-on voltage is considerably smaller (V_{ON} = –5 V) whereas the effective mobility is significantly larger (1.5 $cm^2V^{-1}s^{-1}$) for the OFETs with Au/F4-TCNQ contacts in relation to the reported Au/MoO_x devices.[1] In particular, from the transfer characteristic curves of Figure 6b the switch-on voltage and mobility values obtained were V_{ON} = –13 V and μ = 0.45 $cm^2V^{-1}s^{-1}$ for the device with Au/MoO_x and V_{ON} = –2.1 V and μ = 0.94 $cm^2V^{-1}s^{-1}$ for the device with Au/F4-TCNQ. Output characteristics are shown in Figure S6 in the Supporting Information.

The increase in the effective mobility using F4-TCNQ in the contacts is due to a reduction of the contact resistance as we will show next by analyzing the CPD profiles (Figure 6c). With Au/F4-TCNQ contacts, as a consequence of the similar voltage drop in both source and drain

electrodes, the obtained resistances are very similar ($R_C \cdot W$=5.5 kΩ·cm and $R_C \cdot W$=2.1 kΩ·cm for drain and source contacts, respectively) and significantly lower by about one order of magnitude than those extracted for the Au/MoO_x electrodes. The estimated channel resistance ($R_{CH} \cdot W$ = 0.88 Ω·cm) is comparable to that of the devices with Au/MoOx electrodes, in agreement with a channel free of dopants. The role of contact doping has been widely studied, with the overall injection improvement being attributed to a thinning of the depletion region (thus allowing tunneling injection) and to the reduction of traps density in the metal-semiconductor interface.[45,46,48,49]

The effect of the contacts can be excluded to obtain the intrinsic field-effect mobility along the channel in the linear regime, considering $V_{SD} << V_{SG}-V_{TH}$:[50–52]

$$\mu_{ch} = \left[\frac{I_D L}{W C_i}\right] \frac{1}{\Delta V_{CH}(V_{SG}-V_{TH})} \qquad (2)$$

Where ΔV_{CH} is the voltage drop along the channel, $\Delta V_{CH}=V_{SD}-\Delta V_S-\Delta V_D$, with ΔV_S and ΔV_D the potential drops determined from the CPD profiles at the source and drain contacts, respectively. For the Au/F4-TCNQ device the extracted channel mobility (i.e. excluding the influence of the contacts) is μ_{ch} =10 ± 1 $cm^2\ V^{-1}s^{-1}$. Such a high channel mobility has been reported for C8-BTBT single-crystal devices fabricated by the inkjet-printing method,[53] evidencing the high crystalline quality and the good connectivity between domain boundaries in the 4:1 ratio film prepared by BAMS.

CONCLUSIONS

By means of a microscopic characterization that combines tribologic (FFM) and electrostatic (KPFM) measurements we have deciphered the vertical structure of thin C8-BTBT:PS blend films with nanometer precision for three different C8-BTBT:PS ratios. We have also established

the correlation between the stratified structure and the local electronic response of the OFETs. The films consist of a C8-BTBT crystalline layer sandwiched between two PS layers, one at the bottom and an ultra-thin skin PS layer on the top. We have confirmed that these PS layers improve the OFET stability, as they impede the C8-BTBT films dewetting through time. The thickness of the C8-BTBT layer depends on the blend composition ratio. In particular, the thinnest and laterally incomplete film is found for the 1:2 blend and the thickest film formed by three complete molecular layers, for the 4:1 blend. The investigation of the electronic properties at the nanoscale by KPFM in operando OFETs reveals that the thickness and continuity of the C8-BTBT layer play a fundamental role in the transport channel formation and, herewith, in the overall performance of the devices. KPFM also demonstrates that contact resistance is the critical factor limiting the devices performance, which is significantly improved by doping the contacts with F4-TCNQ. By excluding the contact resistance, a hole mobility in the channel as high as μ_{ch} ~10cm^2 V^{-1}s^{-1} for the OFET with 4:1 ratio was obtained, giving evidence of the excellent transport properties of the film. The optimization of the contacts makes it feasible to reach hole mobility values in high throughput solution processed thin films close to those reported for single-crystal C8-BTBT-based devices.

ASSOCIATED CONTENT

Supporting information: Optical images of the different ratio devices, additional topographic and lateral force AFM data of the studied films, output characteristic of the devices, topographical, excitation and CPD maps obtained by KPFM.

ACKNOWLEDGMENT

This work has been supported by the ERC StG 2012-306826 e-GAMES, Networking Research Center on Bioengineering, Biomaterials, and Nanomedicine (CIBER-BBN), the Generalitat de Catalunya (2014-SGR-17 and 2014- SGR-501) and the Spanish Government under projects MAT2013-47869-C4-1-P, MAT2016-77852-C2-1-R and FANCY CTQ2016-80030-R. We acknowledge the MINECO project MAT2015-68994-REDC and the ‘‘Severo Ochoa’’ Program for Centers of Excellence in R&D (SEV-2015-0496). I.T. and A.P.-R. are enrolled in the Materials Science PhD program of Universitat Autònoma de Barcelona and I.T. acknowledges FPU fellowship from the Spanish Ministry.

REFERENCES

(1) Temiño, I.; Del Pozo, F. G.; Ajayakumar, M. R.; Galindo, S.; Puigdollers, J.; Mas-Torrent, M. A Rapid, Low-Cost, and Scalable Technique for Printing State-of-the-Art Organic Field-Effect Transistors. *Adv. Mater. Technol.* **2016**, 1600090.

(2) Horowitz, G. Organic Field-Effect Transistors. *Adv. Mater.* **1998**, *10*, 159.

(3) Mas-Torrent, M.; Rovira, C. Novel Small Molecules for Organic Field-Effect Transistors:

Towards Processability and High Performance. *Chem. Soc. Rev.* **2008**, *37*, 827–838.

(4) Diao, Y.; Shaw, L.; Bao, Z.; Mannsfeld, S. C. B. Morphology Control Strategies for Solution-Processed Organic Semiconductor Thin Films. *Energy Environ. Sci.* **2014**, *7*, 2145–2159.

(5) Virkar, A. A.; Mannsfeld, S.; Bao, Z.; Stingelin, N. Organic Semiconductor Growth and Morphology Considerations for Organic Thin-Film Transistors. *Adv. Mater.* **2010**, *22*, 3857–3875.

(6) Lee, W. H.; Lim, J. A.; Kwak, D.; Cho, J. H.; Lee, H. S.; Choi, H. H.; Cho, K. Semiconductor-Dielectric Blends: A Facile All Solution Route to Flexible All-Organic Transistors. *Adv. Mater.* **2009**, *21*, 4243–4248.

(7) Paterson, A. F.; Treat, N. D.; Zhang, W.; Fei, Z.; Wyatt-Moon, G.; Faber, H.; Vourlias, G.; Patsalas, P. A.; Solomeshch, O.; Tessler, N.; Heeney, M.; Anthopoulos, T. D. Small Molecule/Polymer Blend Organic Transistors with Hole Mobility Exceeding 13 Cm V−1 s−1. *Adv. Mater.* **2016**, *28*, 7791–7798.

(8) Del Pozo, F. G.; Fabiano, S.; Pfattner, R.; Georgakopoulos, S.; Galindo, S.; Liu, X.; Braun, S.; Fahlman, M.; Veciana, J.; Rovira, C.; Crispin, X.; Berggren, M.; Mas-Torrent, M. Single Crystal-like Performance in Solution-Coated Thin-Film Organic Field-Effect Transistors. *Adv. Funct. Mater.* **2016**, *26*, 2379–2386.

(9) Ford, M. J.; Wang, M.; Patel, S. N.; Phan, H.; Segalman, R. A.; Nguyen, T. Q.; Bazan, G. C. High Mobility Organic Field-Effect Transistors from Majority Insulator Blends. *Chem. Mater.* **2016**, *28*, 1256–1260.

(10) He, D.; Zhang, Y.; Wu, Q.; Xu, R.; Nan, H.; Liu, J.; Yao, J.; Wang, Z.; Yuan, S.; Li, Y.; Shi, Y.; Wang, J.; Ni, Z.; He, L.; Miao, F.; Song, F.; Xu, H.; Watanabe, K.; Taniguchi, T.; Xu, J.-B.; Wang, X. Two-Dimensional Quasi-Freestanding Molecular Crystals for High-Performance Organic Field-Effect Transistors. *Nat. Commun.* **2014**, *5*, 5162.

(11) Niazi, M. R.; Li, R.; Li, E. Q.; Kirmani, A. R.; Abdelsamie, M.; Wang, Q.; Pan, W.; Payne, M. M.; Anthony, J. E.; Smilgies, D.-M.; Thoroddsen, S. T.; Giannelis, E. P.; Amassian, A. Solution-Printed Organic Semiconductor Blends Exhibiting Transport Properties on Par with Single Crystals. *Nat. Commun.* **2015**, *6*, 8598.

(12) Yuan, Y.; Giri, G.; Ayzner, A. L.; Zoombelt, A. P.; Mannsfeld, S. C. B.; Chen, J.; Nordlund, D.; Toney, M. F.; Huang, J.; Bao, Z. Ultra-High Mobility Transparent Organic Thin Film Transistors Grown by an off-Centre Spin-Coating Method. *Nat. Commun.* **2014**, *5*, 3005.

(13) Bobbert, P.; Sharma, A.; Mathijssen, S.; Kemerink, M.; De Leeuw, D. Operational Stability of Organic Field-Effect Transistors. *Adv. Mater.* **2012**, *24*, 1146–1158.

(14) Ohe, T.; Kuribayashi, M.; Yasuda, R.; Tsuboi, A.; Nomoto, K.; Satori, K.; Itabashi, M.; Kasahara, J. Solution-Processed Organic Thin-Film Transistors with Vertical Nanophase Separation. *Appl. Phys. Lett.* **2008**, *93*, 286.

(15) Shin, N.; Kang, J.; Richter, L. J.; Prabhu, V. M.; Kline, R. J.; Fischer, D. A.; Delongchamp, D. M.; Toney, M. F.; Satija, S. K.; Gundlach, D. J.; Purushothaman, B.; Anthony, J. E.; Yoon, D. Y. Vertically Segregated Structure and Properties of Small Molecule-Polymer Blend Semiconductors for Organic Thin-Film Transistors. *Adv. Funct. Mater.* **2013**, *23*, 366–376.

(16) Schweicher, G.; Lemaur, V.; Niebel, C.; Ruzié, C.; Diao, Y.; Goto, O.; Lee, W.; Kim, Y.; Arlin, J.; Karpinska, J.; Kennedy, A. R.; Parkin, S. R.; Olivier, Y.; Mannsfeld, S. C. B.; Cornil, J.; Geerts, Y. H.; Bao, Z. Bulky End-Capped [1]Benzothieno[3,2-B]benzothiophenes: Reaching High-Mobility Organic Semiconductors by Fine Tuning of the Crystalline Solid-State Order. *Adv. Mater.* **2015**, *27*, 3066–3072.

(17) Ebata, H.; Izawa, T.; Miyazaki, E.; Takimiya, K.; Ikeda, M.; Kuwabara, H.; Yui, T. Highly Soluble [1]Benzothieno[3,2- B]Benzothiophene (BTBT) Derivatives for High-Performance, Solution-Processed Organic Field-Effect Transistors. *J. Am. Chem. Soc.* **2007**, *129*, 15732–15733.

(18) Amin, A. Y.; Khassanov, A.; Reuter, K.; Meyer-Friedrichsen, T.; Halik, M. Low-Voltage Organic Field Effect Transistors with a 2-Tridecyl[1]benzothieno[3,2-b][1]benzothiophene Semiconductor Layer. *J. Am. Chem. Soc.* **2012**, *134*, 16548–16550.

(19) Gbabode, G.; Dohr, M.; Niebel, C.; Balandier, J.-Y.; Ruzié, C.; Négrier, P.; Mondieig, D.; Geerts, Y. H.; Resel, R.; Sferrazza, M. X-Ray Structural Investigation of Nonsymmetrically and Symmetrically Alkylated [1]Benzothieno[3,2-B]benzothiophene Derivatives in Bulk and Thin Films. *ACS Appl. Mater. Interfaces* **2014**, *6*, 13413–13421.

(20) Horcas, I.; Fernández, R.; Gómez-Rodríguez, J. M.; Colchero, J.; Gómez-Herrero, J.; Baro, A. M. WSXM: A Software for Scanning Probe Microscopy and a Tool for Nanotechnology. *Rev. Sci. Instrum.* **2007**, *78*, 13705.

(21) Carpick, R. W.; Salmeron, M. Scratching the Surface: Fundamental Investigations of Tribology with Atomic Force Microscopy. *Chem. Rev.* **1997**, *97*, 1163–1194.

(22) Carpick, R. W.; Sasaki, D. Y.; Burns, A. R. Large Friction Anisotropy of a Polydiacetylene Monolayer. *Tribol. Lett.* **1999**, *7*, 79–85.

(23) Glatzel, T.; Lux-Steiner, M. C. C.; Strassburg, E.; Boag, A.; Rosenwaks, Y. Principles of Kelvin Probe Force Microscopy. In *Scanning Probe Microscopy: Electrical and Electromechanical Phenomena at the Nanoscale*; Kalinin, S., Gruverman, A., Eds.; Springer New York: NY, 2007; pp 113–131.

(24) Paradinas, M.; Garzón, L.; Sanchez, F.; Bachelet, R.; Amabilino, D. B.; Fontcuberta, J.; Ocal, C. Tuning the Local Frictional and Electrostatic Responses of Nanostructured SrTiO3—surfaces by Self-Assembled Molecular Monolayers. *Phys. Chem. Chem. Phys.* **2010**, *12*, 4452–4458.

(25) Jones, A. O. F.; Geerts, Y. H.; Karpinska, J.; Kennedy, A. R.; Resel, R.; Röthel, C.; Ruzié, C.; Werzer, O.; Sferrazza, M. Substrate-Induced Phase of a [1]Benzothieno[3,2-B]benzothiophene Derivative and Phase Evolution by Aging and Solvent Vapor Annealing. *ACS Appl. Mater. Interfaces* **2015**, *7*, 1868–1873.

(26) Tsutsumi, J.; Matsuoka, S.; Inoue, S.; Minemawari, H.; Yamada, T.; Hasegawa, T. N-Type Field-Effect Transistors Based on Layered Crystalline Donor–acceptor Semiconductors with Dialkylated Benzothienobenzothiophenes as Electron Donors. *J. Mater. Chem. C* **2015**, *3*, 1976–1981.

(27) Campione, M.; Trabattoni, S.; Moret, M. Nanoscale Mapping of Frictional Anisotropy. *Tribol. Lett.* **2012**, *45*, 219–224.

(28) Hisada, K.; Knobler, C. M. Friction Anisotropy and Asymmetry Related to the Molecular

Tilt Azimuth in a Monolayer of Glycerol Ester. *Langmuir* **2000**, *16*, 9390–9395.

(29) Paradinas, M.; Munuera, C.; Silien, C.; Buck, M.; Ocal, C. Heterogeneous Nanotribological Response of Polymorphic Self-Assembled Monolayers Arising from Domain and Phase Dependent Friction. *Phys. Chem. Chem. Phys.* **2013**, *15*, 1302–1309.

(30) Perez-Rodriguez, A.; Barrena, E.; Fernández, A.; Gnecco, E.; Ocal, C. A Molecular–scale Portrait of Domain Imaging in Organic Surfaces. *Nanoscale* **2017**, *9*, 5589–5596.

(31) Choi, J. S.; Kim, J.; Byun, I.-S.; Lee, D. H.; Lee, M. J.; Park, B. H.; Lee, C.; Yoon, D.; Cheong, H.; Lee, K. H.; Son, Y.; Park, J. Y.; Salmeron, M. Friction Anisotropy Driven Domain Imaging on Exfoliated Monolayer Graphene. *Science (80-.).* **2011**, *333*, 607–610.

(32) Miranzo, P.; López-Mir, L.; Román-Manso, B.; Belmonte, M.; Osendi, M. I.; Ocal, C. Prominent Local Transport in Silicon Carbide Composites Containing in-Situ Synthesized Three-Dimensional Graphene Networks. *J. Eur. Ceram. Soc.* **2016**, *36*, 3073–3081.

(33) Aghamohammadi, M.; Rödel, R.; Zschieschang, U.; Ocal, C.; Boschker, H.; Weitz, R. T.; Barrena, E.; Klauk, H. Threshold-Voltage Shifts in Organic Transistors Due to Self-Assembled Monolayers at the Dielectric: Evidence for Electronic Coupling and Dipolar Effects. *ACS Appl. Mater. Interfaces* **2015**, *7*, 22775–22785.

(34) Aghamohammadi, M.; Fernández, A.; Schmidt, M.; Pérez-Rodríguez, A.; Goñi, A. R.; Fraxedas, J.; Sauthier, G.; Paradinas, M.; Ocal, C.; Barrena, E. Influence of the Relative Molecular Orientation on Interfacial Charge-Transfer Excitons at Donor/acceptor Nanoscale Heterojunctions. *J. Phys. Chem. C* **2014**, *118*, 14833–14839.

(35) Munuera, C.; Barrena, E.; Ocal, C. Scanning Force Microscopy Three-Dimensional

Modes Applied to Conductivity Measurements through Linear-Chain Organic SAMs. *Nanotechnology* **2007**, *18*, 125505.

(36) Leggett, G. J.; Brewer, N. J.; Chong, K. S. L. Friction Force Microscopy: Towards Quantitative Analysis of Molecular Organisation with Nanometre Spatial Resolution. *Phys. Chem. Chem. Phys.* **2005**, *7*, 1107–1120.

(37) Georgakopoulos, S.; del Pozo, F. G.; Mas-Torrent, M. Flexible Organic Transistors Based on a Solution-Sheared PVDF Insulator. *J. Mater. Chem. C* **2015**, *3*, 12199–12202.

(38) Tello, M.; Chiesa, M.; Duffy, C. M.; Sirringhaus, H. Charge Trapping in Intergrain Regions of Pentacene Thin Film Transistors. *Adv. Funct. Mater.* **2008**, *18*, 3907–3913.

(39) Yamagishi, Y.; Noda, K.; Kobayashi, K.; Yamada, H. Interlayer Resistance and Edge-Specific Charging in Layered Molecular Crystals Revealed by Kelvin-Probe Force Microscopy. *J. Phys. Chem. C* **2015**, *119*, 3006–3011.

(40) Bürgi, L.; Sirringhaus, H.; Friend, R. H. Noncontact Potentiometry of Polymer Field-Effect Transistors. *Appl. Phys. Lett.* **2002**, *80*, 2913–2915.

(41) Bürgi, L.; Richards, T. J.; Friend, R. H.; Sirringhaus, H. Close Look at Charge Carrier Injection in Polymer Field-Effect Transistors. *J. Appl. Phys.* **2003**, *94*, 6129–6137.

(42) Liu, C.; Xu, Y.; Noh, Y. Contact Engineering in Organic Field-Effect Transistors. *Biochem. Pharmacol.* **2015**, *18*, 79–96.

(43) Mei, Y.; Fogel, D.; Chen, J.; Ward, J. W.; Payne, M. M.; Anthony, J. E.; Jurchescu, O. D. Interface Engineering to Enhance Charge Injection and Transport in Solution-Deposited Organic Transistors. *Org. Electron.* **2017**, *50*, 100–105.

(44) Kano, M.; Minari, T.; Tsukagoshi, K. Improvement of Subthreshold Current Transport by Contact Interface Modification in P -Type Organic Field-Effect Transistors. *Appl. Phys. Lett.* **2009**, *94*, 101.

(45) Minari, T.; Darmawan, P.; Liu, C.; Li, Y.; Xu, Y.; Tsukagoshi, K. Highly Enhanced Charge Injection in Thienoacene-Based Organic Field-Effect Transistors with Chemically Doped Contact. *Appl. Phys. Lett.* **2012**, *100*, 59.

(46) Tietze, M. L.; Burtone, L.; Riede, M.; Leo, K. Fermi Level Shift and Doping Efficiency in P -Doped Small Molecule Organic Semiconductors : A Photoelectron Spectroscopy and Theoretical Study. *Phys. Rev. B* **2012**, *86*, 35320.

(47) Georgakopoulos, S.; Perez-Rodriguez, A.; Campos, A.; Temiño, I.; Galindo, S.; Barrena, E.; Ocal, C.; Mas-Torrent, M. Spray-Coated Contacts from an Organic Charge Transfer Complex Solution for Organic Fi Eld-Effect Transistors. *Org. Electron.* **2017**, *48*, 365–370.

(48) Natali, D.; Caironi, M. Charge Injection in Solution-Processed Organic Field-Effect Transistors: Physics, Models and Characterization Methods. *Adv. Mater.* **2012**, *24*, 1357–1387.

(49) Hou, J.; Kasemann, D.; Widmer, J.; Günther, A. A.; Lüssem, B.; Leo, K.; Hou, J.; Kasemann, D.; Widmer, J.; Alrun, A. G.; Leo, K. Reduced Contact Resistance in Top-Contact Organic Field-Effect Transistors by Interface Contact Doping. *Appl. Phys. Lett.* **2016**, *108*, 103303.

(50) Natali, D.; Fumagalli, L.; Sampietro, M.; Natali, D.; Fumagalli, L.; Sampietro, M.

Modeling of Organic Thin Film Transistors : Effect of Contact Resistances. *J. Appl. Phys.* **2007**, *101*, 14501.

(51) Gupta, D.; Katiyar, M.; Gupta, D. Mobility Estimation Incorporating the Effects of Contact Resistance and Gate Voltage Dependent Mobility in Top Contact Organic Thin Film Transistors. *Proc. ASID* **2006**, 425–428.

(52) Bittle, E. G.; Basham, J. I.; Jackson, T. N.; Jurchescu, O. D.; Gundlach, D. J. Mobility Overestimation due to Gated Contacts in Organic Field-Effect Transistors. *Nat. Commun.* **2016**, *7*, 10908.

(53) Minemawari, H.; Yamada, T.; Matsui, H.; Tsutsumi, J.; Haas, S.; Chiba, R.; Kumai, R.; Hasegawa, T. Inkjet Printing of Single-Crystal Films. *Nature* **2011**, *475*, 364–367.

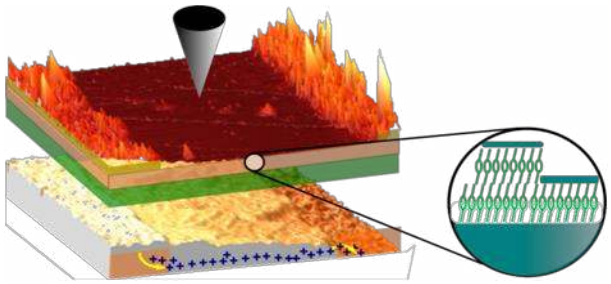

TOC